LAWRENCE
LIVERMORE
NATIONAL
LABORATORY

UCRL-CONF-222365

Rapidly Reconfigurable All-Optical Universal Logic Gates

L. L. Goddard, J. S. Kallman, T. C. Bond

June 23, 2006

SPIE Optics East
Boston, MA, United States
October 1, 2006 through October 4, 2006

Disclaimer

Rapidly Reconfigurable All-Optical Universal Logic Gates

Lynford L. Goddard*, Jeffrey S. Kallman, and Tiziana C. Bond
Lawrence Livermore National Laboratory, 7000 East Avenue, L-223, Livermore, CA 94550

ABSTRACT

We present designs and simulations for a highly cascadable, rapidly reconfigurable, all-optical, universal logic gate. We will discuss the gate's expected performance, e.g. speed, fanout, and contrast ratio, as a function of the device layout and biasing conditions. The gate is a three terminal on-chip device that consists of: (1) the input optical port, (2) the gate selection port, and (3) the output optical port. The device can be built monolithically using a standard multiple quantum well graded index separate confinement heterostructure laser configuration. The gate can be rapidly and repeatedly reprogrammed to perform any of the basic digital logic operations by using an appropriate analog electrical or optical signal at the gate selection port. Specifically, the same gate can be selected to execute one of the 2 basic unary operations (NOT or COPY), or one of the 6 binary operations (OR, XOR, AND, NOR, XNOR, or NAND), or one of the many logic operations involving more than two inputs. The speed of the gate for logic operations as well as for reprogramming the function of the gate is primarily limited to the small signal modulation speed of a laser, which can be on the order of tens of GHz. The reprogrammable nature of the universal gate offers maximum flexibility and interchangeability for the end user since the entire application of a photonic integrated circuit built from cascaded universal logic gates can be changed simply by adjusting the gate selection port signals.

Keywords: Photonic integrated circuits, optical logic, gain-index lever, sampled grating DBR, alternating facet laser

1. INTRODUCTION

Efficient, high-speed, single transverse mode, all-optical gates with positive inverter gain and a reasonably large contrast ratio are needed for on-chip digital photonic logic circuits. Positive inverter gain, a.k.a. high fanout, is the ability to shut off a strong optical signal using a weaker input signal. It is needed in order to cascade logic gates without introducing external amplifiers. Contrast is the ratio of the output power when the digital output represents 1 to when it represents 0. It is a key factor in determining signal noise margins and strongly affects bit error rates. Numerous solutions involving changing the reflection or transmission of off-chip normally incident light have been proposed and demonstrated [1-3]. State of the art on-chip research has primarily focused on optical gain quenching and/or optical bistability in a multiple section device [4-8]. Various approaches and strategies have included using: (1) a pre-amplifier to boost the weaker input signal, (2) the gain lever effect to enhance gain quenching, (3) a saturable absorber to induce bistability and accelerate gain quenching and (4) carrier induced non-linear effects. To our knowledge, each on-chip approach or combination of approaches to date has significant performance tradeoffs among efficiency, speed, single mode operation, inverter gain, and contrast ratio. These tradeoffs are unavoidable in devices that use optical gain quenching or optical bistability because when the laser is quenched below threshold, it takes an incredibly long time to turn back on. This time constant is related to the carrier lifetime, and thus limits the operation to speed to about 1GHz. Partial quenching solutions may increase the speed to 5-10GHz, but obviously at the expense of signal contrast. Also, hysteresis loops in bistable devices can cause ambiguity and increase bit error rates. Another fundamental problem is that gain quenching is optimal just above transparency ($N_c^{ideal} \approx e \cdot N_{tr}$, where $e = 2.718$) due to the competing effects of increasing stimulated emission and decreasing differential gain with bias, whereas the device speed increases with bias. Gain quenched devices tend to have their highest inverter gain just above threshold, which is where they are slowest.

To solve these problems, we have designed a new type of on-chip semiconductor device. The rapidly reconfigurable all-optical universal logic gate combines some existing technologies and several new innovations together to achieve its novel functionality. This paper, which describes the device design and performance, is divided into 8 sections. In Section 2, we introduce a method to achieve universal logic functionality from a single gate. Sections 3 through 5 discuss the underlying physics that we will use to implement this method. We present simulation results in Section 6, discuss the performance of the device in Section 7, and give concluding remarks in Section 8.

* goddard5@llnl.gov; phone 1 925 424-2341; fax 1 925 423-7085

2. A METHOD FOR UNIVERSAL LOGIC OPERATIONS

We will present the device schematics with a top-down overview. The overarching goal is to create a device with a layout as shown in Figure 1 that is capable of generating an output power versus input power as shown in Figure 2.

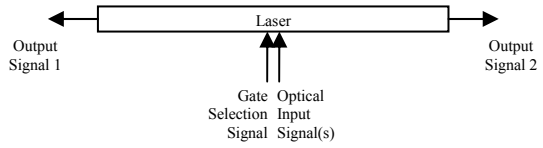

Figure 1: Simplistic block diagram of a universal logic gate.

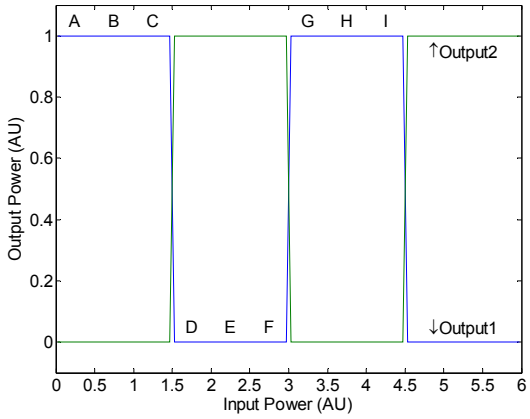

Figure 2: Ideal characteristics for the output power from output ports 1 (blue) and 2 (green) as a function of total input power. The scale is the same for vertical and horizontal axes. Each on or off pulse is ideally 1.5 units wide and the letters from A through I are uniformly spaced by 0.5 units.

Applying an analog gate selection signal translates the curves in Figure 2 to the left and thereby selects a particular gate operation. For instance, a 1.25 unit continuous selection signal would center label C on the vertical axis and select XNOR operation at output port 1. Then, input of two digital bits (0 or 1 unit each) would put the operation point at C = on for 00 input, E = off for 01 or 10, and G = on for 11. In a similar manner, a 1.75 unit selection signal centers label D and selects AND operation since the input would put the operation at D = off for 00, F = off for 01 or 10, and H = on for 11. The correspondence between letters and binary gate operation is A = NAND, B = NOR, C = XNOR, D = AND, E = OR, and F = XOR. The necessary selection signals are 0.25, 0.75, 1.25, 1.75, 2.25, and 2.75 units, respectively. The correspondence between letters and unary gate operations are B or C = NOT and E or F = COPY since a NOT gate is the same as a NOR or XNOR gate with one of the inputs set to 0 and a COPY gate is the same as an OR or XOR gate with one of the inputs set to 0. Two full periods of the periodic power dependence, as shown in Figure 2, are sufficient to cover all logic operations. This transfer function is very similar to the one discovered independently by Hurtado et. al. [9], but here, we use digital input bits of the same amplitude for all logic operations, which improves cascadability.

To achieve the periodic power dependence goal, we will use a two step approach. The first step is to design specialized wavelength dependent mirrors. At certain wavelengths, which correspond to half of the Fabry-Perot modes, the left facet has a high reflectivity (R>40%) while the right facet has a low reflectivity (R<2%) so that almost all of the circulating laser power is output from the right side, i.e. output 2. At other wavelengths, which correspond to the other half of the longitudinal modes, the right facet has a high reflectivity while the left facet has a low reflectivity so that the laser light is output from the left side, i.e. output 1. The second step is to devise a layout such that a small input optical signal efficiently shifts the dominant lasing mode to the next adjacent mode. We will combine a novel effect, the gain-index lever, with the well-known Vernier effect to accomplish this objective. Previous research has discussed how the gain lever can be used to enhance the carrier induced refractive index change and thereby increase the tuning rate of DFB lasers [10]. Here, we will discuss how to realize a true index lever to further amplify the already enhanced refractive index change and how to use the Vernier effect to significantly reduce the necessary tuning signal.

3. MIRROR DESIGN

Sampled grating (SG) or superstructure grating (SSG) distributed Bragg reflectors (DBRs) are two excellent choices to realize our desired reflectivity properties. One can perform computer aided design simulations to engineer the superstructure gratings that give the perfect reflectivity profiles. For simplicity, we will discuss sampled gratings since the design and performance properties of SG-DBR lasers are described extensively in [11]. The main result of the paper is that one can produce a comb of reflectivity peaks with a specific spacing and amplitude envelope by using a periodically sampled continuous grating. We will build on their results to calculate the necessary gratings for our design, which has the additional requirement of alternating output facets. We will assume a design wavelength, λ_d = 980nm, but operation at other wavelengths, e.g. 1310nm or 1550nm is a simple matter of rescaling device dimensions and changing the materials of various device layers. The laser gain peak is assumed to be at 980nm. Figure 3 shows the refractive index profile and simulated reflectivity spectra for two mirrors that are symmetrically offset from λ_d to have central wavelengths of λ_1 = 981.09nm and λ_2 = 978.92nm.

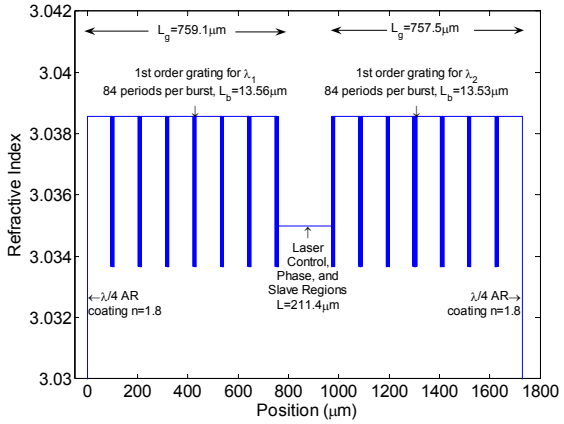

Figure 3a: Refractive index profile. Each mirror has 7 grating bursts (κ = 100cm^{-1}) with a 12.5% burst duty cycle. The mirrors are symmetrically offset from λ = 980nm to have central wavelengths λ_1 = 981.09nm and λ_2 = 978.92nm and are $L_{g1} = 4704\lambda_1/2n_r \approx 759.1\mu m$ and $L_{g2} = 4704\lambda_2/2n_r \approx 757.5\mu m$ long, respectively.

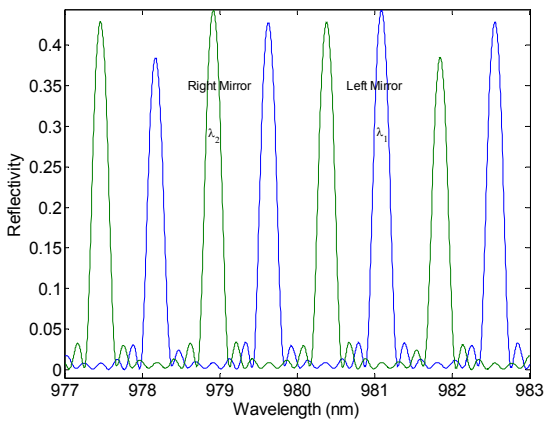

Figure 3b: Simulated reflectivity versus wavelength for mirrors 1 (blue) and 2 (green).

Each mirror has 7 grating bursts (κ = 100cm^{-1}) with a 12.5% burst duty cycle and a single layer quarter wave anti-reflective coating ($n_r \approx 1.8$) prior to the air interface. The total mirror grating lengths are an integral number of half wavelengths, $L_{g1,g2} = m\lambda_{1,2}/2n_r$ with m = 4704, yielding $L_{g1} \approx 759.1\mu m$ and $L_{g2} \approx 757.5\mu m$. The choice of $m = 4704 = 2^5 \cdot 3 \cdot 7^2$ arose from the requirement that the length of each grating section must be an integral number of half wavelengths. Thus, m must be divisible by 56 since there are 7 grating bursts and the burst duty cycle is 1:8. This leads to 84 grating periods per grating burst and burst lengths of $L_{b1} \approx 13.56\mu m$ and $L_{b2} \approx 13.53\mu m$. The factors in 4704 allowed us to study the effects of different duty cycles, e.g. 1:4, 1:6, 1:7, 1:8, 1:16, and numbers of grating bursts, e.g. 3, 4, 6, 7, 12, while maintaining a constant mirror length. The 7 grating bursts generate exactly 7-2 = 5 local maxima between the major comb peaks. The central wavelengths were coarsely chosen so that each major peak occurs at the same wavelength as the smallest of these local maxima and so that there are exactly two major peaks, at λ = 979.64 and 980.37nm, of slightly lower amplitude between the design wavelengths peaks. This generates 4 modes with the same net round-trip gain, $G = \Gamma g - \alpha_i - \alpha_m$, as shown in Figure 4 since the slightly weaker reflectivity peaks have slightly higher material gain. The central wavelengths are then finely tuned so that the wavelength separation between these 4 adjacent maxima in the net gain spectrum is constant. This ensures three important features. First, there are exactly 4 evenly spaced wavelengths that have maximum net gain and all other peaks have lower net gain. Thus, the device will tend to lase in only one of these four modes. Second, the reflectivity ratio at these wavelengths is enormous and so the laser light is output almost entirely from the low reflectivity facet. Third, the high and low reflectivity facets alternate for

adjacent peaks. In Figure 3, the facet reflectivities are around 44% and 0.91%. Thus, 92% of the laser light is output the low reflectivity facet (contrast ratio ≈ 11dB) since [12]:

$$\frac{P_2}{P_1} = \frac{1-R_2}{1-R_1}\sqrt{\frac{R_1}{R_2}} \tag{1}$$

where P_1 and P_2 are the emitted powers and R_1 and R_2 are the reflectivities of mirrors 1 and 2, respectively.

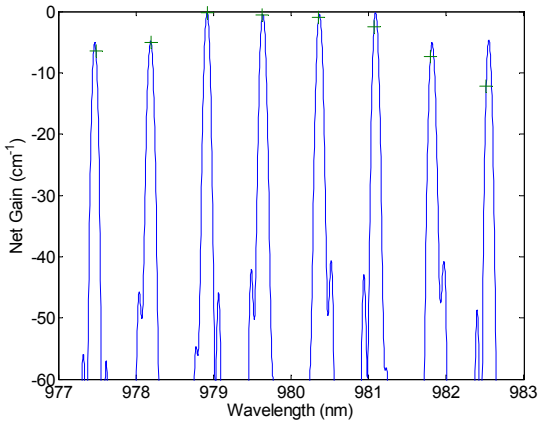

Figure 4: Round-trip net gain, $G=\Gamma g-\alpha_i-\alpha_m$, versus wavelength for a 211.4μm long laser with sampled grating DBR mirrors of Figure 3. Constructive interference locations are denoted by a green cross. The laser is designed so that the central 4 modes have the same net gain and so that they dominate over all other modes. At this particular bias, which corresponds to N_c = $2.8\text{x}10^{18}\text{cm}^3$ and $N_s = 10.9\text{x}10^{18}\text{cm}^3$, the mode at 978.92nm has the highest net gain and will be the dominant mode.

Figure 4 shows the net gain profile for a 211.4μm long laser with the mirrors described in figure 3. The choice of laser length will be explained later. A green cross denotes a location that satisfies the round trip in-phase requirement (constructive interference). The cross with the highest round trip gain will be the dominant laser mode since clearly it will experience the most amplification. We are currently developing a steady state and time dependent model of the expected power distribution for the competing longitudinal modes, but believe that most of the circulating power will belong to a single mode and that there will still be some laser power in one or two adjacent longitudinal modes.

One complication inherent in all-optical cascadable device is that the device should respond to the input signals but be insensitive to the resulting changes. In electro-optical systems, this is easy since the input signal can be electrical which distinguishes it from the circulating optical signal. In non-cascadable all-optical systems, this is also easy since the wavelengths can be different. In our case, the wavelengths are the same and further, when the lasing mode changes, the asymmetric circulating power profile changes drastically. This change is usually much larger than the input signal that created the change to begin with. To solve this problem, we propose using a narrow region at the middle of the laser length for the input because the amplitude of the circulating light in the very center of the laser is unchanged when the output facet switches. Two other optional tricks to make the input light intensity stronger than the circulating light intensity while still maintaining a single mode output are: (1) circulating the input light by reflecting it a fixed number of times across the input region and (2) making the laser a multimode interferometer with single mode output tapers at each end. The first trick increases the effective input light intensity while the second trick decreases the circulating light intensity in the input region without changing the output power. These two tricks will also increase the fanout of the device. Another issue is that the mirrors must be non-absorbing to prevent their reflectivities from shifting. This can be accomplished either by biasing them at transparency or by using quantum well intermixing to blueshift the bandgap [13]. The tradeoff for the two solutions is between requiring additional current controls or additional wafer processing steps. However, the quantum well intermixing approach can also solve the problem of unwanted carrier diffusion between electrically isolated sections.

4. THE GAIN-INDEX LEVER

We begin our explanation of the gain-index lever by first describing the ordinary gain lever effect. Consider a laser with electrically isolated sections (control and slave) as shown in Figure 5.

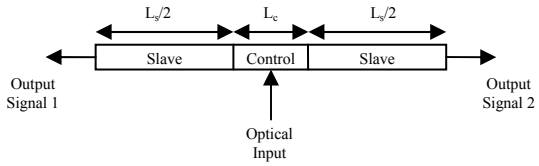

Figure 5: Laser with an electrically isolated control section in the center of a longer slave region. Optical input at control section reduces the control carrier density and causes the slave carrier density to increase. The power at each facet decreases.

The slave sections are biased to a high carrier density, N_s, while the control section to a moderate carrier density, N_c. Both sections are above transparency, N_{tr}, and experience gain. Stimulated emission from a side input optical signal reduces the carrier density in the control section. The round-trip gain is now less than the loss and so the circulating optical power decreases. Since the circulating power decreases, the carrier density of the slave section begins to increase until the round-trip gain equal loss condition is re-established. However, due to the sub-linear gain versus carrier density relationship, the slave carrier density increase is enhanced compared to the control density decrease. Specifically [14],

$$L_s \frac{\partial g}{\partial N_s} \Delta N_s = -L_c \frac{\partial g}{\partial N_c} \Delta N_c \tag{2a}$$

$$\therefore \Delta N_s = -\frac{L_c}{L_s} \frac{\partial g / \partial N_c}{\partial g / \partial N_s} \Delta N_c \tag{2b}$$

This is the well-known gain lever effect, whereby a small change in N_c results in a large change in N_s, and is the basis for previous state of the art on-chip inverter research. For reasons to be explained later, we define an enhancement factor, or gain lever, to only include the ratio of the differential gains, i.e.,

$$GL \equiv \frac{\partial g / \partial N_c}{\partial g / \partial N_s} = \frac{N_s}{N_c} \tag{3}$$

where we have assumed a logarithmic gain versus carrier density relationship [15] to evaluate the differential gains. It appears that the gain lever can be made arbitrarily large by reducing the control section density. However, when the device is lasing, the circulating laser power will pump the control section and increase the density to transparency. Thus, the maximum gain lever is N_s/N_{tr}.

To understand the gain-index lever effect, consider the wavelength shift caused by the carrier induced change to the optical path length of the laser from above. Lasing not only requires that the round-trip gain equals the loss, but also that the round-trip phase be an integer multiple of 2π (constructive interference). The refractive index (mode index) of the laser decreases with carrier density and so the wavelengths that experience constructive interference (green crosses in Figure 4) shift with carrier density. To maintain constructive interference, the change in the round-trip optical path length must be zero:

$$0 = \Delta\phi_{rt} = \Delta\left[4\pi\frac{(n_r^c L_c + n_r^s L_s)}{\lambda}\right] \tag{4a}$$

$$\therefore \Delta\lambda = \frac{\lambda}{n_r^c L_c + n_r^s L_s}\frac{\partial n_r^c}{\partial N_c} L_c \Delta N_c\left(1 - \frac{\alpha_s}{\alpha_c}\right) \tag{4b}$$

where n_r^c and n_r^s and α_c and α_s are the refractive indices and linewidth enhancement factors for the control and slave sections, respectively; note that we have used Equation 2b to evaluate ΔN_s in terms of ΔN_c. The linewidth enhancement factor for the control section for example is given by $\alpha_c = -4\pi/\lambda\ (\partial n_r^c/\partial N_c)/(\partial g/\partial N_c)$. Note that the refractive indices of the two sections are almost identical, $n_r \approx n_r^c \approx n_r^s$, but that the differential refractive indices can be quite different. Equation 4b represents a blueshift ($\Delta\lambda<0$) if $\alpha_s>\alpha_c$ since $\partial n_r^c/\partial N_c<0$ and $\Delta N_c<0$.

Equation 4b has two interesting consequences. First, we observe that it is possible to directly modulate the laser without any wavelength chirp if we arrange α_s to be equal to α_c. This chirp-free behavior would make these lasers highly desirable as transmitters in dense wavelength division multiplexing (DWDM) applications. Second, the index lever, *IL*, defined as ratio of the wavelength shift for the multi-section device compared to the shift for a one-section device, i.e. no slave sections, is given by:

$$IL \equiv 1 - \frac{\alpha_s}{\alpha_c} \tag{5}$$

Since the linewidth enhancement factors are usually positive, we will need $\alpha_s>2\alpha_c$ to achieve a true index lever ($|IL|>1$), i.e. an enhancement in the wavelength shift. Most lasers have slowly varying linewidth enhancement factors, but Stohs et. al. have shown [16] that a shallow InGaAs well, e.g. a 5.2nm $In_{0.16}Ga_{0.84}As$ single quantum well embedded in a 300nm GaAs barrier/waveguide layer, has a linewidth enhancement factor that varies by a factor of 10. They attribute this huge variation in α to the relative ease of populating barrier states, which contribute significantly to the refractive index but very little to the gain according to the Kramers-Kronig relation. Thus, we can design our device to achieve the full gain-index lever by choosing a barrier material with relatively small band offsets ($\approx 2\text{-}3k_BT$ for ΔE_c and ΔE_v) to the quantum well. For simplicity, we will use the same shallow InGaAs well as Stohs et. al. since linewidth enhancement data is available and the quantum well composition and thickness yield 980nm operation. However, we will need four quantum wells of thickness 5.2nm to increase the optical confinement factor, Γ, to 8.3% to overcome the mirror loss of $131cm^{-1}$. We assume that the linewidth enhancement factor for the four quantum well device will be comparable to the single well device for equal carrier densities.

5. LASER DESIGN

To complete the device, consider now the multi-section device embedded in the wavelength dependent mirrors described by Figure 3. Since the mirror reflectivities vary with wavelength, the mirror loss changes with carrier density. As before, the side input optical signal reduces the carrier density in the control section and thereby decreases the circulating optical power. The slave section carrier density begins to increase, but now, the round-trip gains for the constructive interference locations change because the reflectivity is not constant. The round-trip gain for the dominant mode begins to decrease from its maximum, while the gain for an adjacent mode increases to its maximum. Thus, the dominant laser mode will switch between a left output and a right output mode whenever these round-trip gains pass each other.

Since the mirror reflectivity is now wavelength dependent, the mirror phase will also vary and so we need to modify Equations 4a and 4b to include the phase changes, ϕ_m^l and ϕ_m^r, for the left and right mirrors, respectively:

$$0 = \Delta\phi_{rt} = \Delta\left[4\pi\frac{(n_r^c L_c + n_r^s L_s)}{\lambda} + \phi_m^l + \phi_m^r\right] \tag{6a}$$

$$\therefore \Delta\lambda = \frac{\lambda}{n_r^c L_c + n_r^s L_s + n_r^g (L_{eff}^l + L_{eff}^r)} \left(\frac{\partial n_r^c}{\partial N_c} L_c \Delta N_c \right) IL \tag{6b}$$

where L_{eff}^{l} and L_{eff}^{r} are the effective mirror lengths defined by [17]:

$$L_{eff} \equiv \frac{\lambda^2}{4\pi n_r} \frac{\partial \phi}{\partial \lambda} \tag{7}$$

Note that L_{eff} is highly wavelength dependent because the phase derivative varies considerably. Thus, the size of the wavelength shift of a constructive interference location, i.e. $\Delta\lambda$ in Equation 6b, depends on its location in the reflectivity spectrum. For a weakly reflecting continuous DBR grating, the effective length of 1 mirror near the Bragg frequency (central maximum) is half the total grating length, i.e. $L_{eff}^{l} = L_g/2$. However, the effective length is shorter for a sampled grating DBR. For the sampled grating described by Figure 3, we find that near each central maximum $L_{eff}^{l} \approx L_g/3 \approx 253\mu m$ but near the smallest local maximum the effective length is reduced to $L_{eff}^{l} \approx L_g/6 \approx 126\mu m$. More interesting is that the effective length is <u>negative</u> in the vicinity of local reflectivity minima and that the effective length averaged between adjacent central maxima of the same mirror is about half the burst length, $L_{eff\,avg}^{l} \approx L_b/2 \approx 6.75\mu m$.

To estimate the carrier density changes needed for switching, it is useful to rewrite Equation 6b in a dimensionless form by normalizing it to the average mode spacing for constructive interference, $MS = \lambda^2/(2n_r L_{avg})$:

$$\frac{\Delta\lambda}{MS} = \left[\frac{L_{avg}}{L_{local}} \right] \left(\frac{2}{\lambda} \frac{\partial n_r^c}{\partial n_c} L_c \Delta N_c \right) IL \tag{8}$$

where $L_{avg} = L_c+L_s+L_{eff\,avg}^{l}+L_{eff\,avg}^{r}$ and $L_{local} = L_c+L_s+L_{eff}^{l}+L_{eff}^{r}$. Note that $L_{eff\,avg}^{l} \approx L_{eff\,avg}^{r} \approx 6.75\mu m$ are constants whereas L_{eff}^{l} and L_{eff}^{r} vary with wavelength. The constructive interference locations undergo a full period of translation when the absolute value of the ratio, $\Delta\lambda/MS$, in Equation 8 increases from zero to one. By definition, $L_{local} = L_{avg}$ when averaged over 1 translation period. We estimate we would need $\Delta N_c = -6.25x10^{18}cm^3$ to achieve a full switching cycle translation given typical device parameters such as $L_c = 40\mu m$, IL = -2.5, and $\partial n_r^c/\partial N_c = -\Gamma(1x10^{-20}cm^3) = -8x10^{-22}cm^3$ [18] assuming a confinement factor of $\Gamma = 8\%$. Such a huge carrier density change is not possible especially since the steady state value of N_c is only $\approx 3x10^{18}cm^3$. We could try increasing the control length by a factor of 10 to $L_c = 400\mu m$ to reduce the necessary carrier density to $\Delta N_c = -6.25x10^{17}cm^3$. This will not work because N_c would get reduced to just above transparency to keep the single pass gain of the section unchanged. For the 10x longer section, the section gain will be unchanged if $10 \cdot \ln(N_c^{new}/N_{tr}) = \ln(N_c^{old}/N_{tr})$. Thus, the new control carrier density would be $N_c^{new} = (N_c^{old})^{0.1} N_{tr}^{0.9} = 1.89x10^{18}cm^3$ assuming $N_{tr} = 1.8x10^{18}cm^3$. Even with a powerful input signal, the control section can only decrease to transparency and so the maximum achievable ΔN_c would be $9x10^{16}cm^3$. This is still smaller than the desired $6.25x10^{17}cm^3$. Moreover, it would be impractical to spread the input optical signal over such a wide width.

Fortunately, we can engineer the device to use a Vernier effect so that a much smaller change is needed. For instance, we arranged the constructive interference location spacing to be 1% smaller than the net gain peak location separations in Figure 4. This was accomplished by choosing $L_c+L_s \approx 211.4\mu m$ so that $L_{avg} \approx 224.9\mu m$. The gain peak location separations were approximately given by $\lambda^2/(2n_r L_{eff}^{gp})$ with $L_{eff}^{gp} = L_g/3.41 \approx 222.4\mu m$. The factor 3.41 arises because the reflectivity maximum and smallest local maximum are separated by 3.5 orders, i.e. half of the 7 orders between the comb teeth. Fine tuning of the design wavelengths λ_1 and λ_2 to make the mode spacing constant reduced the target separation to 3.41 orders. With a 1% difference between the mode spacing and the net gain peak spacing, only a 4% total translation of the constructive interference locations is needed to sequentially tune the dominant laser mode through the 4 modes and achieve a full switching cycle, i.e. two full periods or 6 units of input optical power in Figure 2. It turns out that the needed translation is actually larger due to the wavelength dependence of L_{local}. Since $L_{local} \approx 590\mu m$ at the net gain peaks ($L_c+L_s = 211.4\mu m$, $L_{eff}^{l} \approx 253\mu m$, $L_{eff}^{r} \approx 126\mu m$ for a right output mode) and $L_{local} \approx 450\mu m$ for tuning through the 4 net gain peaks, the wavelength tuning is reduced according to Equation 8 by the factor $L_{avg}/L_{local} \approx 0.5$. Thus, we need about 8% translation or $\Delta N_c = 5x10^{17}cm^3$ for $N_c = 3x10^{18}cm^3$ and $L_c = 40\mu m$. Note that

the size of the Vernier effect has to be carefully chosen. The mode spacing and net gain peak spacing must be sufficiently dissimilar so that only a single gain peak is selected to lase.

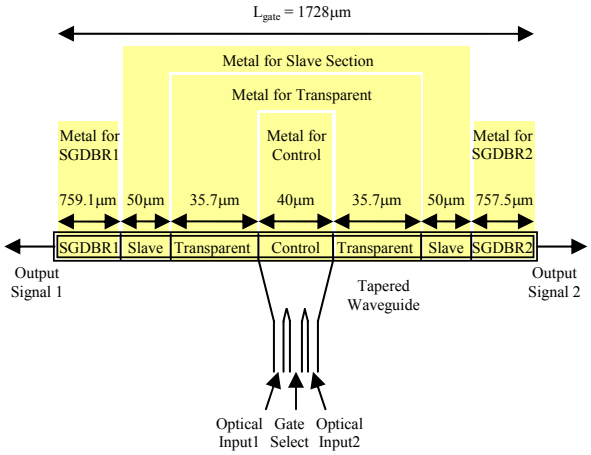

Figure 6: A 2-input port device design layout (not to scale). The double lined box around the laser indicates a ridge waveguide, i.e. mesa structure. The ridge is between 2.5 and 5.0μm wide. The sampled grating distributed Bragg reflectors (SG-DBRs) were described in Figure 3. The digital optical input and analog gate select signals are spread out in a tapered waveguide from their initial size of ≈ 5μm to quench the full 40μm of the control region. Each section along the length is electrically isolated by a 3-4μm gap, which counts as part of the length of the section. The metallization shorts together both sides of the slave section so that they have the identical bias. This ensures that they behave symmetrically when the laser shifts between left and right output modes. The transparent phase control sections are also shorted together. However, since the mirrors are designed to be different, each mirror has its own current source to enable fine tuning capabilities.

Figure 6 shows the complete device design. The analog gate selection port and the one, two, or multiple digital input ports feed into a tapered waveguide that partially quenches the control section. The advantage of the side input waveguide over a facet input waveguide is that on-chip optical isolators are not needed between cascaded gates. In addition to the slave and control section, we added a transparent section to serve two purposes: phase control and index/gain lever strength control. We propose creating this section using quantum well intermixing so that adjusting the bias on the section changes the refractive index but not the gain seen by the laser modes. The intermixed well is blueshifted and thus transparent, but its carriers contribute a noticeable amount to the refractive index, i.e. the intermixed well has a large linewidth enhancement factor. For a fixed control section length and mode spacing, the length of the transparent section is chosen as a function of the desired slave section carrier density. A longer transparent section reduces the slave section length and forces a larger slave carrier density. This increases both the gain lever and index lever, but reduces the wall plug efficiency of the device. Once the length of the transparent section is fixed, adjusting the bias on the section will allow us to align the cavity phase so that we are in the 8% of the tuning range that passes through the 4 modes. Electrical isolation of the various sections is provided by leaving a 3-4μm gap in the metal contact and by heavily intermixing the quantum well underneath the gap to suppress carrier diffusion between sections.

6. SIMULATIONS

Figure 7 shows the simulated wavelength tuning and output power switching when the control section carrier density is reduced from $3.25\text{x}10^{18}$ to $2.75\text{x}10^{18}\text{cm}^3$ (N_s increases from $10.1\text{x}10^{18}$ to $10.9\text{x}10^{18}\text{cm}^3$) for a device with L_c = 40μm, L_s = 100mm and a transparent section with L_p = 71.4μm. We have assumed a logarithmic gain and a constant $\partial n_r^c/\partial N_c = -8\text{x}10^{-22}\text{cm}^3$ over the tuning range so that GL ≈ 3.5 and IL ≈ -2.5. The tuning is independent of the laser ridge width. The green crosses in Figure 4 march to the left along the net gain curve as the control carrier density decreases. As a green cross lines up with a gain peak, that lasing mode is selected and so the laser tunes from λ=981.09nm to 980.37nm to 979.64nm to 978.92nm, sequentially.

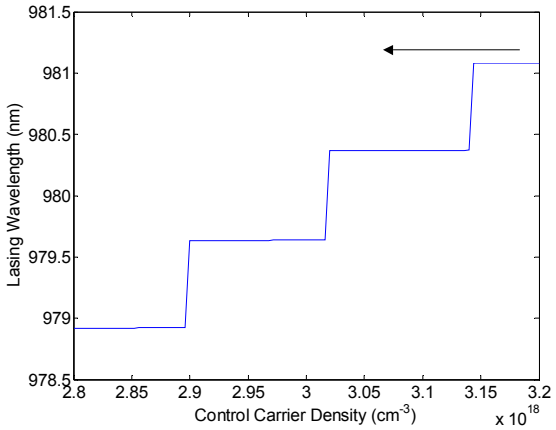

Figure 7a: Simulated tuning as N_c decreases due to optical input. At $3.2x10^{18}cm^3$, the green cross near 981.09nm in Figure 4 was closest to its maximum and thus was the lasing wavelength. As N_c decreases and N_s increases, the resonance conditions blueshifts and the next mode becomes dominant.

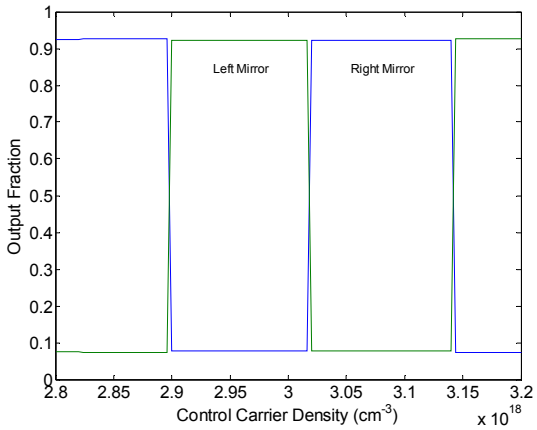

Figure 7b: Output fraction of the dominant lasing mode. As a result of the alternating output facets, the fraction of the laser light that is output a given facet shifts between 8 and 92%. The actual contrast ratio will be lower since the non-dominant modes will still lase at reduced intensities.

Another approach to visualizing the wavelength tuning process is to study the complex-valued, round-trip amplification factor, A, for the electric field,

$$A = |r_l r_r| \exp\left[\frac{\Gamma g - \alpha_i}{2} 2L + i\phi_{rt}\right] \tag{9}$$

where $|r_l|$ and $|r_r|$ are the reflection coefficient magnitudes of the left and right mirrors. Their phase information is lumped into ϕ_{rt}. The electric field gain is half the intensity gain. The round-trip length is 2L. A parametric plot of the amplification factor as the wavelength is stepped is shown in Figure 8 for $N_c = 2.8x10^{18}cm^3$ and $N_s = 10.9x10^{18}cm^3$.

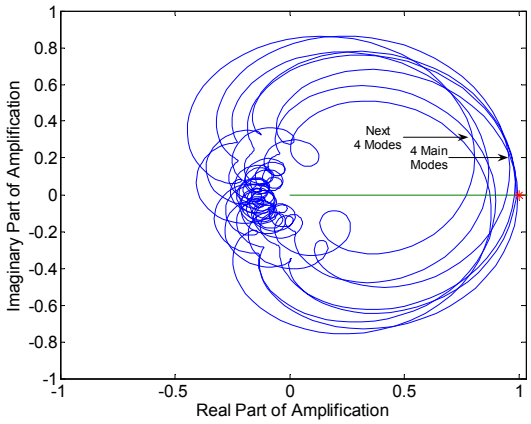

Figure 8: Parametric plot of the round trip electric-field amplification factor, A, in the complex plane for $N_c = 2.8x10^{18}cm^3$ and $N_s = 10.9x10^{18}cm^3$. Constructive interference occurs where the blue curve intersects the green line. The point on the blue curve that is closest to the threshold condition, denoted by the red star, determines the laser wavelength. In the positive real half plane, wavelengths near the four main modes (λ=978.92, 979.64, 980.37, and 981.09nm), form slightly offset half ellipses that are closer to the lasing threshold condition than wavelengths near the next four modes (λ=977.47, 978.19, 981.82, and 982.55nm). Optical input changes the carrier densities and causes the blue curve to rotate counter clockwise as N_c is reduced.

There is constructive interference whenever the blue curve intersects the green line on the positive real axis. The threshold condition of Re(amplification) = 1, Im(amplification) = 0 is denoted by the red asterisk. The point on the blue curve that is closest to the red asterisk is the dominant laser mode. In the positive real half plane, the wavelengths that are near the four dominant modes (λ=978.92, 979.64, 980.37, and 981.09nm), form slightly offset half ellipses that are closer to the lasing threshold condition than the wavelengths that are near the next four modes (λ=977.47, 978.19, 981.82, and 982.55nm). As the carrier densities are tuned, the total gain remains constant, but the round-trip phase varies. Thus, the entire amplification shape simply rotates counter clockwise about the origin. With the Vernier effect, we only need the blue curve to make a small rotation to make each of the four modes be closest to the threshold condition rather than needing an entire 2π rotation.

A separate 1-dimensional rate equation simulation was conducted for the four quantum well laser where each well was 5.2nm thick and the applied current densities for the control and slave section were set to J_c = 1.5kA/cm^2 and J_s = 7.2kA/cm^2 to achieve the aforementioned carrier densities. The current densities of 1.5 and 7.2kA/cm^2 may seem high, but when normalized by the number of quantum wells they are quite reasonable. They would correspond to 375 and 1800A/cm^2 in Figure 14 of Stohs paper [16]. We found that the output power of the 2.5μm wide device under these conditions is 8mW and that the necessary input power to achieve the ΔN_c of 5x10^{17}cm^3 is 40mW. Thus, 1 unit of optical input power corresponds to 40mW/6units = 6.67mW and so the device has a fanout of 8mW/6.67mW = 1.2. A 5μm wide device should still lase in a single transverse mode, provide 16mW of output power, and require the same 40mW of input power to get ΔN_c = 5x10^{17}cm^3, i.e. a fanout of 2.4, assuming fixed current densities. This may not seem like a high fanout, but 5μm wide by 200μm long side-input gain quenched devices have typical fanouts that are below 0.25. For these current densities, the operation current would be 19.5mA for the 2.5μm wide device assuming that the mirrors and transparent phase control sections do not need biasing to correct for manufacturing errors. Assuming the device has a series resistance of 10Ω, the drive voltage would be 1.46V. Thus, the wall plug efficiency would be 28%. Gain quenched devices with comparable contrast ratios and fanouts have to operate near threshold and typically have efficiencies under 5%.

For either width, the speed of our device for the 40mW input signal appears to be about 2GHz since the carrier density change of 5x10^{17}cm^3 is not really a small signal modulation and moreover, the relaxation oscillation frequency is only 4GHz. A smaller input signal generates a smaller modulation and thus a response speed that is closer to the resonance frequency. For example, a 13mW input signal (2 units) gives a device response of about 3GHz. Thus, the gate operation speed would be 3GHz, while the gate reprogramming speed would be slightly less than 3GHz since the gate operations have smaller input signals (0, 1, or 2 units) compared to gate selection signals (0-3 units). To get to operation at tens of GHz, as promised in the abstract, the relaxation oscillation frequency must be increased. The resonance frequency, f_r, is approximately given by [19],

$$f_r \approx \frac{1}{2\pi}\sqrt{v_g \frac{\partial g}{\partial N}\frac{S_0}{\tau_p}} \tag{10}$$

where v_g is the group velocity, S_0 is the circulating photon density, and τ_p is the photon cavity lifetime. Since these parameters vary from section to section, the overall resonance frequency will be an average of these parameters along the device length. We can increase f_r, by increasing S_0 or $\partial g/\partial N$ or by decreasing τ_p by reducing the mirror reflectivities. Increasing S_0 will increase P_{out}, but it will also make changing ΔN_c harder since the input signal has to compete with a stronger circulating signal. Increasing the current densities to J_c = 1.75kA/cm^2 and J_s = 8kA/cm^2 increased the circulating intensity by 28%, the resonance frequency by 14%, and the necessary input power by 13%. Thus, faster operation with higher fanout is possible at higher output powers; moreover, the contrast ratio will increase slightly since the mode suppression ratio generally increases with increasing power [20]. Increasing the average differential gain will reduce the strength of the gain and index levers, but might be tolerable since we can trade some of the high fanout in the 5μm device for speed. If we decrease τ_p, we will need to decrease the length of the transparent section L_p and increase L_s to maintain a constant slave carrier density. In other words, we can trade ease of phase control for increased speed. In summary, we should surpass 10GHz operation by increasing the output power and optimizing for speed instead of high fanout and ease of operation.

7. DISCUSSION OF RESULTS

To increase the output coupling fraction (i.e. contrast ratio), we would like to increase the number of grating bursts so that the reflectivity at the smallest local maximum is reduced. However, as the number of grating bursts increases, the sampled grating DBR behaves more like a continuous DBR and the effective length increases to $L_g/2$ at the central maximum as well as at the smallest local maximum. Thus, a higher ΔN_c is needed to achieve a given wavelength shift. Thus, there is a tradeoff between necessary input power for switching and contrast ratio since both increase with the number of grating bursts.

It is desirable that the output signal amplitude (vertical scale of Figure 2) be slightly more than 1 unit high in order to compensate for waveguide and interface losses. This is the case for the 2.5μm wide device, which has a fanout of 1.2. Since the left and right outputs are digital negations of each other, the effective fanout is actually double if we design half of the downstream gates to work using complementary logic, i.e. deMorgan's Laws. For some gates, such as clock source distribution nodes or gates that drive several logic stages in a cascaded circuit, high fanout is necessary, i.e. a 10-unit output signal or preferably ten 1-unit output signals. The periodic power dependence shown in Figure 2, which is vital for achieving a universal gate, implies that a 2 unit input signal would act similar to a 0 unit signal. Thus, high power signals require splitting and/or using attenuators or threshold cutoff gates to reduce the signal back down to 1 unit amplitude before being used in downstream gates.

As mentioned previously, the gain or fanout of the gate can be increased by reflecting the input light a fixed number of times across the control region and/or by making the laser a multimode interferometer (MMI) with single mode output tapers at each end. Figure 9a shows a layout that uses both techniques to increase the fanout to 19.6 from 1.2 for the simple 2.5μm wide gate. The input light now makes a double pass across the control region, which effectively doubles the input power. Also, the MMI allows the laser width to be increased to 20.4μm, which increases the output power.

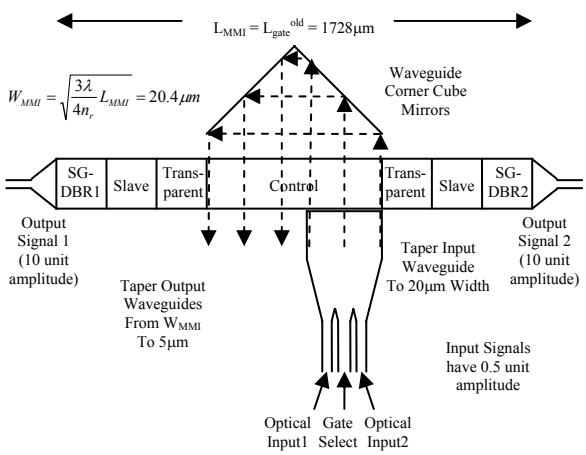

Figure 9a: High fanout MMI design with two input passes. The fanout is 19.6. In the MMI design, there is a narrow 1-2μm gap with AR coated surfaces between the tapered waveguide and the control section to reduce the perturbation of the MMI's rectangular shape due to the waveguide input.

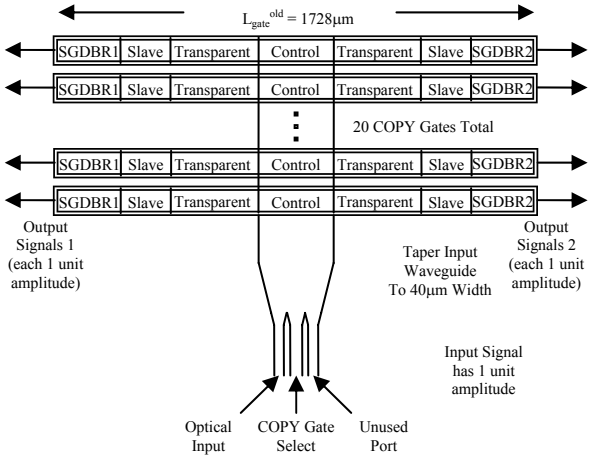

Figure 9b: High fanout design that reuses the same input signal to drive multiple COPY gates in parallel. The fanout is 20 and the outputs are naturally normalized to 1 unit signals for immediate use in downstream gates.

An alternative strategy to achieving high fanout is simply to make multiple copies of the input signal. This can be accomplished by reusing the input signal to drive many COPY gates in parallel as shown in Figure 9b. We assume that the gain for the input signal when traversing each gate compensates for waveguide and interface losses. Under this assumption, the gates act as a signal splitter with built in amplitude regeneration. This technique has two major advantages over the MMI layout with multi-pass input. First, the production will be simpler since the corner cube

mirrors and MMIs do not have to be fabricated. Each COPY gate is programmed using a generic universal logic gate. Second, dedicated splitting elements and amplitude regulators do not have to be fabricated. The outputs are already normalized to the correct 1 bit amplitude. Thus, the multiple COPY gate approach is the better approach for high fanout applications. Every optical element in the circuit will be manufactured identically and functionality of sub-circuit modules will be determined by their layout and gate selection signals.

For reliable operation of this high sensitivity device, the ambient conditions and input signals need to be very precisely controlled and the manufacturing tolerances are very tight. Each bin in Figure 2 is denoted by a letter and has a width of 0.5 units. Thus, when we center a bin, we can tolerate a total of ±0.25 units of noise. For a 2 input gate, we can distribute this noise budget according to: ±0.05 units per input signal, ±0.05 units for the gate selection signal, ±0.05 units for uniformity of the bin widths (i.e. the power needed to go from C to F might differ from the power for F to I), ±0.05 units for temperature fluctuations and ±0.025 units each for drive current fluctuations in the slave and control sections. For the input signal (0 or 1 unit), this means we can tolerate ±5% intensity noise. For the gate selection signal (0-3 units), we can tolerate ±1.66% intensity noise. The temperature dependence of the refractive index for (In)GaAs is approximately 2×10^{-4} per °C [21] and the coefficient of thermal expansion of the GaAs substrate is 5.8ppm per °C [22]. This corresponds to a wavelength redshift of the reflectivity spectrum of 0.070nm per °C since $L_g = m\lambda/2n_r$ implies that $\Delta\lambda/\lambda = \Delta n_r/n_r + \Delta L/L$. Fortunately, the constructive interference locations will redshift at the same rate. However, the calculated bandgap redshift of the $In_{0.16}Ga_{0.84}As$ quantum well is 0.32nm per °C [23] and so the gain peak redshifts relative to the reflectivity peaks at a rate of 0.25nm per °C. Thus, the gate would cycle through the four modes (2.17nm separation) if the temperature changed by 8.68°C. This change is approximately equivalent to 6 units of input optical power. Therefore, the device will need to be mounted epitaxial side down on a heatsink with an active temperature controller capable of better than ±0.072°C long-term stability to achieve less than ±0.05 units of temperature fluctuations. The control carrier density changes by ≈ 13% and the slave density by ≈ 6% during the tuning with 6 units of power. Thus, we would need to control their densities to better than 540ppm and 250ppm. Naively, the current control would need to be about this good, although the sub-linear carrier density versus current density relationship should give us extra breathing room. Commercial laser controllers that meet these tight specifications are readily available, e.g. the ILX-Lightwave LDT-5948 temperature controller has a guaranteed accuracy and long term stability of better than ±0.005°C and the LDX-3525 laser driver has a typical accuracy and long term stability of better than ±250ppm.

The sensitivity of the gate to temperature and bias current can be used to compensate for slight manufacturing errors. Active temperature control can be used to coarsely align the gain peak of the wafer with the mirror reflectivity spectrum. Fine alignment to compensate for wafer non-uniformity can be performed on each gate or region of gates by slight adjustments of the biases on each mirror and on the control, slave, and transparent sections. With such a large number of degrees of freedom, the operating conditions that produce the output power versus input power curves closest to the ideal cases in Figure 2 can be found using a suitable gradient search technique.

8. CONCLUSION

In summary, the rapidly reconfigurable all-optical universal logic gate is a versatile high-speed generic on-chip photonic device. The same gate can perform a complete set of logic operations as well as provide numerous additional functionality [24], e.g. wavelength conversion, signal duplication, threshold switching, analog to digital conversion, digital to analog conversion, and signal routing. The gate utilizes the gain-index lever and Vernier effect to shift the laser between left and right output facet modes. Since the laser remains well above threshold during the mode switching process, operation at high-speed (tens of GHz) with high contrast ratio (>10dB) and wall-plug efficiency (>25%) is feasible from a single mode device.

REFERENCES

1. A. Walker, "Application of bistable optical logic gate arrays to all-optical digital parallel processing," *Applied Optics*, **25**, pp. 1578-1585 (May 1986).

2. A. Lentine, H. Hinton, D. Miller, J. Henry, J. Cunningham, and L. Chirovsky, "Symmetric Self-Electrooptic Effect Device: Optical Set-Reset Latch, Differential Logic Gate, and Differential Modulator/Detector," *IEEE J. Quantum Electron.*, **25**, pp. 1928-1936 (Aug 1989).
3. G. Boyd, D. Miller, D. Chemla, S. McCall, A. Gossard, and J. English, "Multiple quantum well reflection modulator," *Appl. Phys. Lett.*, **50**, 1119-1121 (Apr 1987).
4. M. Takenaka and Y. Nakano, "Realization of All-Optical Flip-Flop Using Directionally Coupled Bistable Laser Diode," *IEEE Photon. Technol. Lett.*, **16**, pp. 45-47 (Jan 2004).
5. J. Zhou, M. Cada, and T. Makino, "All-Optical Bistable Switching Dynamics in 1.55-μm Two-Segment Strained Multiquantum-Well Distributed-Feedback Lasers," *IEEE J. Lightwave Technol.*, **15**, pp. 342-55 (Feb 1997).
6. M. Okada, H. Kikuchi, K. Takizawa, and H. Fujikake, "The Effects of a Detuned Optical Input on Bistable Laser Diodes with Inhomogenerous Current Injection," *IEEE J. Quantum Electron.*, **29**, pp. 109-120 (Jan 1993).
7. H. Nobuhara, K. Kondo, S. Yamakoshi, and K. Wakao, "Optical Logic Functions Using a Tunable Wavelength Conversion Laser Diode," *IEEE J. Quantum Electron.*, **28**, pp. 1722-1726 (Jul 1992).
8. M. Jinno, and T. Matsumoto, "Nonlinear Operations of 1.55-μm Wavelength Multielectrode Distributed-Feedback Laser Diodes and Their Applications for Optical Signal Processing," *IEEE J. Lightwave Technol.*, **10**, pp. 448-457 (Apr 1992).
9. A. Hurtado, A. Gonzalez-Marcos, and J.A. Martin-Pereda, "All-Optical Logic Gates with 1550nm Fabry-Perot and Distributed Feedback Semiconductor Laser Amplifiers," *Electron Devices, 2005 Spanish Conf. on Electron Devices*, pp. 305-308 (Feb 2005).
10. G. Griffel, R. Lang, and A. Yariv, "Two-Section Gain-Levered Tunable Distributed Feedback Laser with Active Tuning Section," *IEEE J. Quantum Electron.*, **30**, pp. 15-18 (Jan 1994).
11. V. Jayaraman, Z. Chuang, and L. Coldren, "Theory, Design, and Performance of Extended Tuning Range Semiconductor Lasers with Sampled Gratings," *IEEE J. Quantum Electron.*, **29**, pp. 1824-1834 (June 1993).
12. H. Shimizu, K. Kumada, S. Uchiyama, and A. Kasukawa, "Extremely large differential gain of 1.26μm GaInNAsSb-SQW ridge lasers," *Electron. Lett.*, **37**, pp. 28-30 (Jan 2001).
13. J. Marsh, S. Hansen, A. Bryce, R. De La Rue, "Applications of neutral impurity disordering in fabricated low-loss optical waveguides and integrated waveguide devices," *Opt. Quant. Electron.*, **23**, pp. S941-S957 (Jan 1991).
14. K. Vahala, M. Newkirk, and T. Chen, "The optical gain lever: A novel gain mechanism in the direct modulation of quantum well semiconductor lasers," *Appl. Phys. Lett.*, **54**, pp. 2506-2508 (June 1989).
15. L. Coldren and S. Corzine, Diode Lasers and Photonic Integrated Circuits (Wiley, New York, 1995), 1st ed., pp. 167.
16. J. Stohs, D. Bossert, D. Gallant, and S. Brueck, "Gain, Refractive Index Change, and Linewidth Enhancement Factor in Broad-Area GaAs and InGaAs Quantum-Well Lasers," *IEEE J. Quantum Electron.*, **37**, pp. 1449-1459 (Nov 2001).
17. L. Coldren and S. Corzine, Diode Lasers and Photonic Integrated Circuits (Wiley, New York, 1995), 1st ed., p. 94.
18. L. Coldren and S. Corzine, Diode Lasers and Photonic Integrated Circuits (Wiley, New York, 1995), 1st ed., p. 101.
19. S. Chuang, Physics of Optoelectronic Devices (Wiley, New York, 1995), 1st ed., pp. 491.
20. L. Coldren and S. Corzine, Diode Lasers and Photonic Integrated Circuits (Wiley, New York, 1995), 1st ed., pp. 106-108.
21. M. Bertolotti, V. Bogdanov, A. Ferrari, A. Jascow, N. Nazorova, A. Pikhtin, and L. Schirone, "Temperature dependence of the refractive index in semiconductors," *J. Opt. Soc. Am. B*, **7**, pp. 918-922 (June 1990).
22. T. Soma, J. Satoh, and H. Matsuo, "Thermal expansion coefficient of GaAs and InP," *Solid State Commun.*, **42**, pp. 889-892 (June 1982).
23. I. Vurgaftman, J. Meyer, and L. Ram-Mohan, "Band parameters for III-V compound semiconductors and their alloys," *J. Appl. Phys.*, **89**, pp. 5815-5875 (June 2001).
24. L. Goddard, J. Kallman, and T. Bond "The Rapidly Reconfigurable All-Optical Universal Logic Gate and Its Applications," to be submitted to *IEEE J. Quantum Electron*.

This work was performed under the auspices of the U.S. Department of Energy by University of California, Lawrence Livermore National Laboratory under Contract W-7405-Eng-48.